

Drift time estimation by dynamic time warping

Tianci Cui and Gary F. Margrave

ABSTRACT

The drift time is the difference between the event time at seismic frequencies and at sonic logging frequencies predicted by the attenuation theory. The synthetic seismogram needs drift time correction to tie the seismic trace. In this report, the drift time is estimated by dynamic time warping (DTW) method, which is based on the constrained optimization algorithm. By matching the stationary and nonstationary seismograms, DTW can estimate the drift time automatically without knowledge of Q or check-shot records. The estimated drift time is caused by apparent Q attenuation and may contain extra time shift due to the phase error in the wavelet used to construct the stationary seismogram. After applying drift time correction to the stationary seismogram, the residual phase between it and the nonstationary seismogram is almost constant in both time and frequencies. Then time-variant amplitude balancing and time-variant or time-invariant constant-phase rotation are applied to the nonstationary seismogram to perfect the matching.

DYNAMIC TIME WARPING

Consider two synthetic seismograms $s_1(n)$ and $s_2(n)$ shown in the Figure 1 top panel where n is sample number. Seismogram $s_1(n)$ is computed by convolving a minimum-phase wavelet with a random reflectivity sequence. Seismogram $s_2(n)$ is obtained by applying a time-varying shift sequence $tdr(n)$ to $s_1(n)$. The maximum crosscorrelation coefficient between $s_1(n)$ and $s_2(n)$ is about 0.41 and this occurs at a lag of -22.4 samples. Time shift sequence $tdr(n)$ is represented by part of a sinusoidal function as shown in Figure 1 bottom panel. Representing the time shift $tdr(n)$ as lag ndr

$$ndr = \text{round}\left(\frac{tdr}{dt}\right), \quad (1)$$

where dt is the time sample interval. Therefore, the two seismograms are related by

$$s_2(n) = s_1(n + ndr(n)). \quad (2)$$

In this report, the dynamic time warping (DTW) method (Hale, 2013) is adapted to estimate the time shift sequence $ndr(n)$ given the seismograms $s_1(n)$ and $s_2(n)$. Then the estimated $ndr(n)$ is applied to $s_1(n)$ by equation 2 so that the two seismograms gain a better correlation with each other.

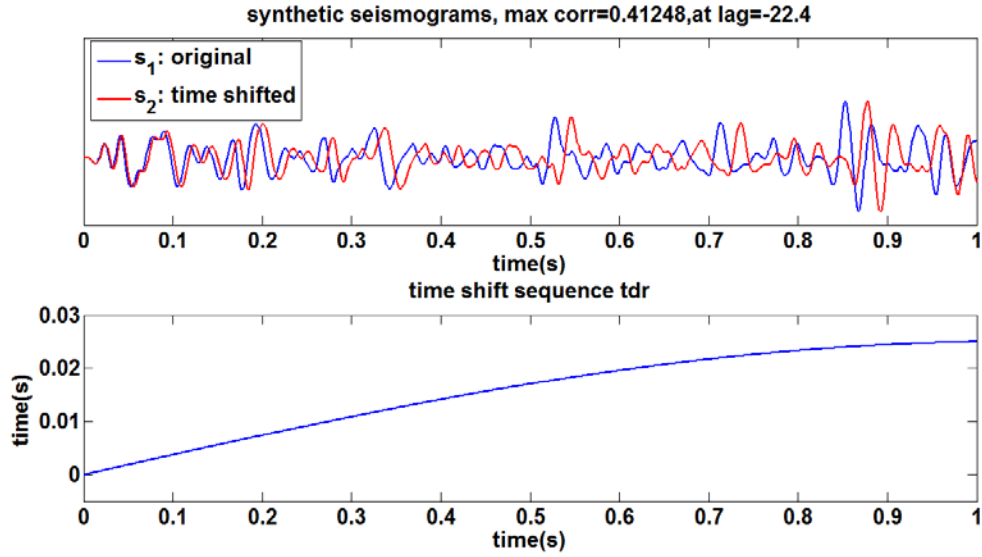


FIG 1: Two synthetic seismograms (top) and the time shift sequence between them (bottom).

To find the lag sequence between two seismograms, an array of *alignment errors* e is calculated according to

$$e(m, n) = [s_1(n) - s_2(n + m)]^2 \quad (3)$$

for all the sample numbers $n = 1, 2, \dots, N$ of s_1 and s_2 . Lag m is set to be $-L \leq m \leq L$, namely for each sample $s_1(n)$, we calculate the squared differences between $s_1(n)$ and the most adjacent $2L + 1$ samples to $s_2(n)$. The alignment error array, computed for the two synthetic seismograms in Figure 1 with $N = 1001$ and $L = 50$, is shown in Figure 2. The red curve is the true lag sequence $ndr(n)$ calculated from $tdr(n)$ by equation 1. Note that the alignment error is nearly zero along the lag sequence $ndr(n)$ where $m(n)$ is approximate to $ndr(n)$. There are 101^{1001} paths along $n = 1, 2, \dots, N$, among which $ndr(n)$ is the one whose cumulative error summing along its path is the smallest. However, calculating 101^{1001} cumulative errors and finding the smallest one is far beyond the computation ability of a modern computer. Fortunately, DTW can solve it by applying suitable constraints to this problem and therefore reduce computation dramatically.

Constrained optimization

DTW computes a sequence $u(n) = [u(1), u(2), \dots, u(N)]$ that closely approximates the known lag sequence $ndr(n) = [ndr(1), ndr(2), \dots, ndr(N)]$ by solving the following optimization problem:

$$u(1 : N) = \arg \min_{m(1:N)} D[m(1 : N)], \quad (4)$$

where

$$D[m(1:N)] = \sum_{n=1}^N e(n, m(n)) \quad (5)$$

subject to the constraint

$$|u(n) - u(n-1)| \leq 1. \quad (6)$$

The function D is referred to as *total distance* which represents the accumulative errors summing along a path from left to right in the alignment error image shown in Figure 2. DTW chooses a path $u(1:N)$ to minimize the total distance from the paths satisfying the constraint required by equation 6, the number of which is about 3^N , much smaller than $(2L+1)^N$ but still too large. The constraint itself indicates that the lag sequence $u(n)$ cannot change too rapidly from one sample to the next, which is reasonable for the drift time sequence. When $u(n) - u(n-1) = 1$, the synthetic seismogram is stretched such that two adjacent samples in s_2 is corresponding to two non-adjacent samples in s_1 with one sample between them. When $u(n) - u(n-1) = -1$, the synthetic is squeezed such that two adjacent samples in s_2 is corresponding to only one sample in s_1 .

Dynamic Programming

DTW is a dynamic programming algorithm, which decomposes a problem into a sequence of smaller and nested subproblems. Consider a subpath $u(1:k)$ of the minimizing path $u(1:N)$, $u(1:k)$ should satisfy

$$u(1:k) = \arg \min_{m(1:k)} \sum_{n=1}^k e(n, m(n)), \quad (7)$$

namely $u(1:n)$ must be a minimizing subpath or $u(1:N)$ could not be minimize D . According to equation 7, we can further decrease the number of paths we will search from 3^N in two steps: accumulation and backtracking.

Accumulation

In the accumulation step, an array of *distances* $d(m, n)$ is computed recursively from the array of alignment errors $e(m, n)$ as follows:

$$d(m, 1) = e(m, 1), \quad (8)$$

$$d(m, n) = e(m, n) + \min \begin{cases} d(m-1, n-1) \\ d(m, n-1) \\ d(m+1, n-1) \end{cases}, \quad n = 2, 3, \dots, N. \quad (9)$$

The distance array calculated from the alignment error array in Figure 2 is shown in Figure 3.

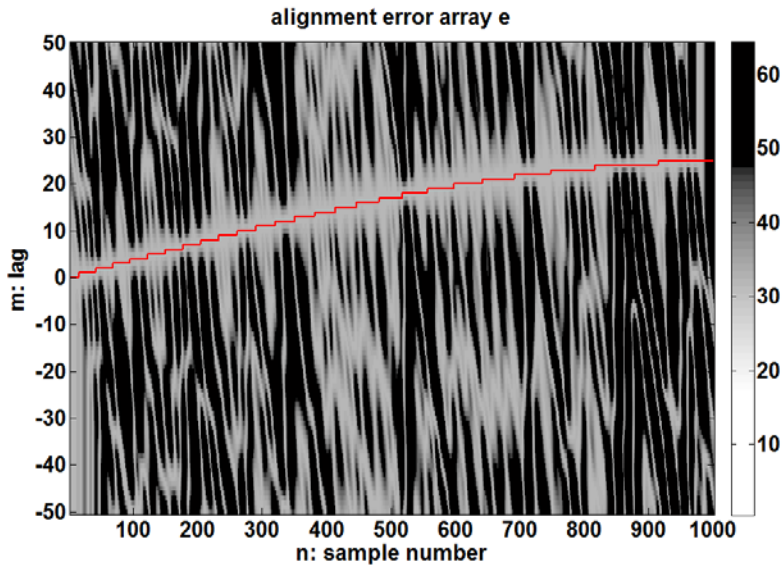


FIG 2: Grayscale background is alignment error array where white color indicates the value of error is zero. The red curve is the known lag sequence from which s_2 is created.

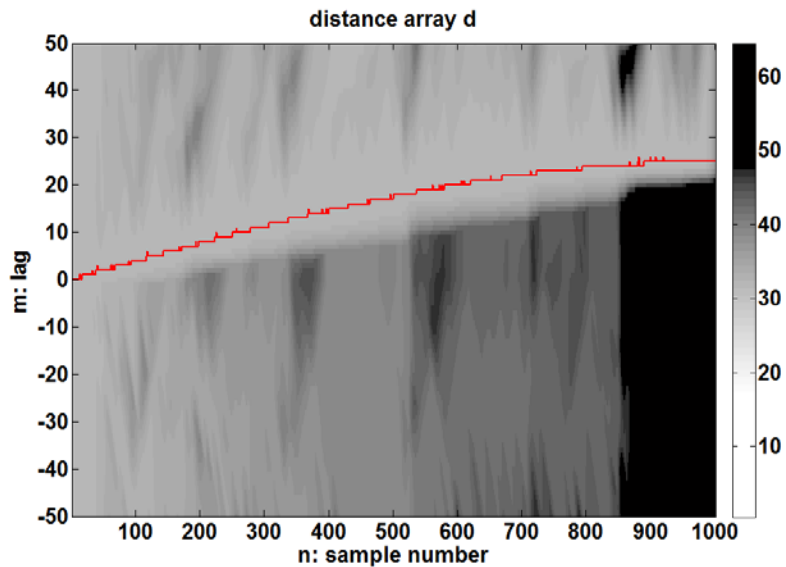


FIG 3: Grayscale background is distance array where white color indicates the value of distance is zero. The red curve is the lag sequence u calculated by DTW.

Backtracking

In the backtracking step we calculate the minimizing path $u(1:N)$ starting with the last lag $u(N)$ and ending with the first lag $u(1)$ as follows:

$$u(N) = \arg \min_{-L \leq m \leq L} d(m, N), \quad (10)$$

$$u(n) = \arg \min_{m \in \{u(n+1)+1, u(n+1), u(n+1)-1\}} d(m, n), \quad n = N-1, N-2, \dots, 1. \quad (11)$$

The computational complexity of the accumulation step is $O((2L+1) \times N)$ and of the backtracking step is $O(N)$, which is easily realized on a personal computer.

The lag sequence $u(n)$ computed by DTW is shown as the red curve in Figure 3. The lag sequence $u(n)$ is represented as time shift sequence $tu(n)$ by

$$tu(n) = u(n) \times dt \quad (12)$$

and plotted in Figure 4 top panel in red with the known time shift sequence $tdr(n)$ in blue. We can observe that the time shift sequence calculated from DTW matches the known time shift sequence quite well. For further study, the calculated time shift sequence $tu(n)$ is applied to s_1 using equation 2 and the corrected seismogram is shown in red in Figure 4 bottom panel in comparison with s_2 in blue. The maximum crosscorrelation coefficient between them is almost 1 at a lag of -0.3 samples.

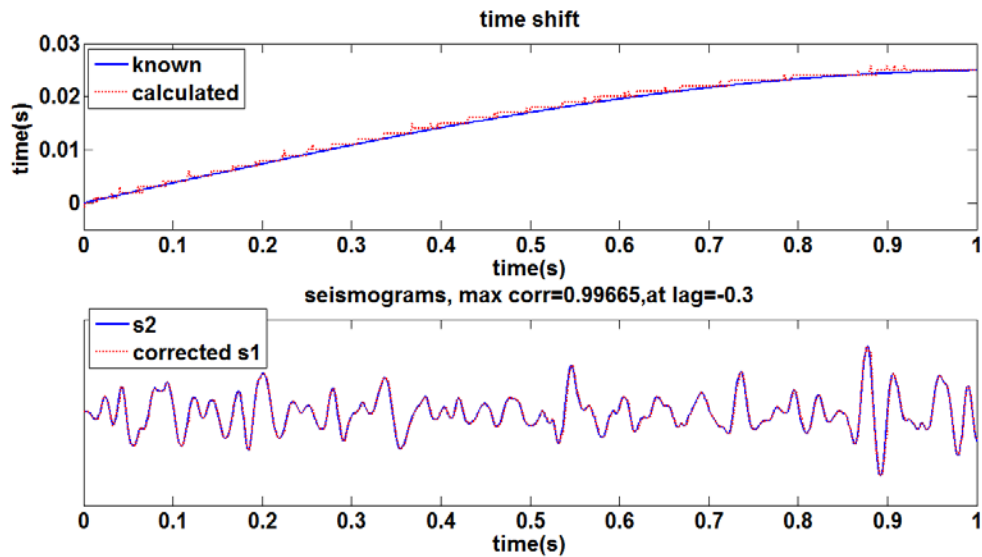


FIG 4: Known and DTW calculated time shift sequences (top). Seismograms s_2 and s_1 after correction using DTW calculated time shift sequence (bottom).

DRIFT TIME ESTIMATION

Drift time

In practice, $s_1(n)$ might be a synthetic seismogram created from well log data, $s_2(n)$ might be a recorded seismic trace, and $tdr(n)$ might be the drift time between $s_1(n)$ and $s_2(n)$. The drift time is the difference between the event time at seismic frequencies and at sonic logging frequencies predicted by the attenuation theory (Margrave, 2013). According to the constant-Q model (Kjartansson, 1979), in which Q is independent of frequency, two monochromatic waves having frequencies f_1 and f_2 respectively will propagate at different wavespeeds $v(f_1)$ and $v(f_2)$, which are related by

$$v(f_2) = v(f_1) \left[1 + \frac{1}{\pi Q} \left(\frac{f_2}{f_1} \right) \right]. \quad (13)$$

The dominant frequency of well logging f_1 is about 12500Hz while the dominant frequency of seismic exploration f_2 is typically below 50 Hz, so the velocities measured by the sonic tool will be systematically faster than those experienced by seismic waves. Given a layered medium, the two-way vertical travelttime is given by

$$t(z_n, f) = 2 \sum_{k=1}^n \frac{dz_k}{v_k(f)} \quad (14)$$

where $dz_k = z_{k+1} - z_k$ is the layer thickness, and $v_k(f)$ is the frequency dependent phase velocity of the k^{th} layer. Thus the drift time is

$$tdr(z_n) = t(z_n, f_2) - t(z_n, f_1). \quad (15)$$

In seismic-to-well ties, the drift time $tdr(n)$ is to be estimated by correlating the synthetic seismogram $s_1(n)$ calculated from well log data to the seismic trace $s_2(n)$ recorded near the well location. Then the synthetic seismogram $s_1(n)$ is tied to the seismic trace $s_2(n)$ by applying $tdr(n)$ to it. In this report, we will use the dynamic time warping (DTW) method as described before to estimate the drift time.

Well-based 1D seismogram model

In Figure 5, a p-sonic log and a density log in depth from Hussar well 12-27 are shown after editing. For simplicity, we assume both logs start from the surface. Using the two logs, the reflectivity in two-way travelttime is calculated. Convolving the reflectivity with a minimum-phase wavelet whose dominant frequency is 30 Hz (Figure 6), a stationary seismogram is created. To include the Q effects in the 1D seismogram, a synthetic zero offset VSP is constructed for the well-log model of Figure 5 using function `vspmodelq` in the CREWES toolbox after Ganley (1981). Figure 7 shows the primary-only upgoing

wavefield with a Q value of 50 and the same wavelet as in Figure 6. The trace recorded at the receiver with a zero depth is essentially the 1D seismogram with Q effects.

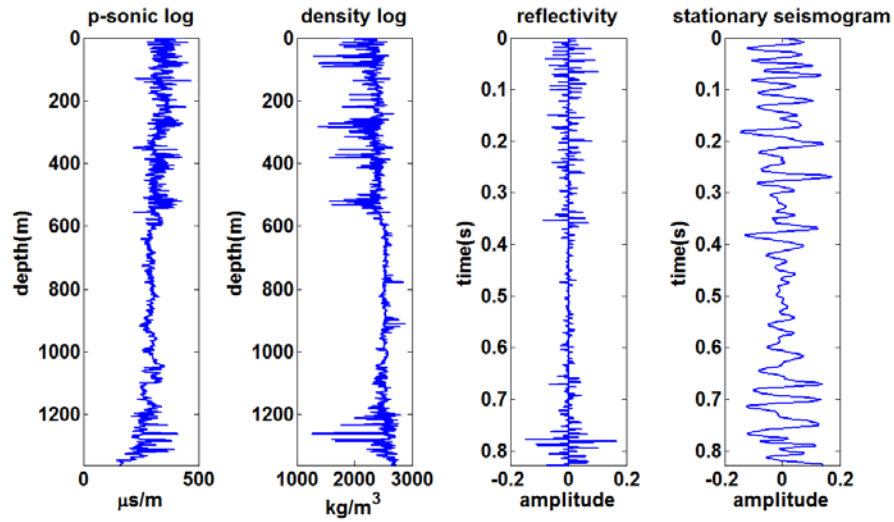


FIG 5: The p-sonic log, density log from Hussar well 12-27 and the resulting reflectivity and stationary seismogram.

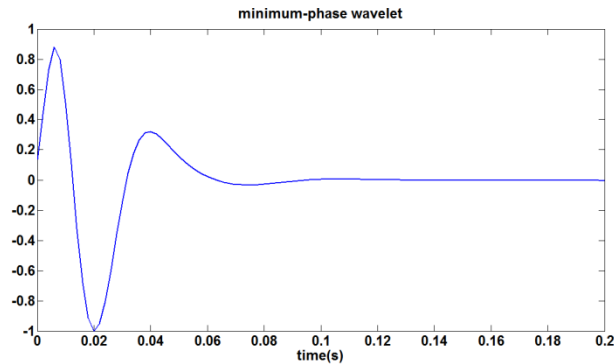


FIG 6: The minimum-phase wavelet with a dominant frequency of 30 Hz for 1D seismogram construction.

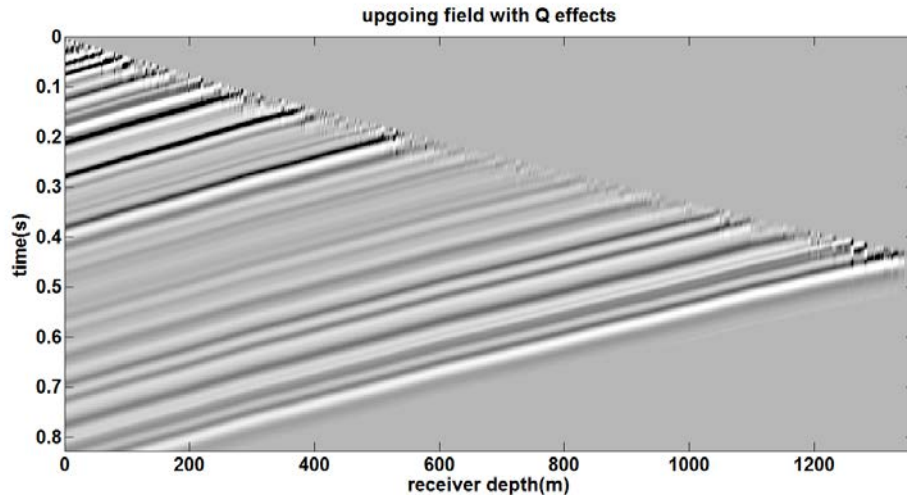


FIG 7: The upgoing wavefield for the VSP modelling without multiples or transmission loss.

Drift time estimation by further constrained DTW

The stationary seismogram in blue and the nonstationary seismogram with Q effects in red are shown in the top panel of Figure 8. The latter shows progressive attenuation indicated by both the diminishing amplitude and the widening wavelets compared to the former. The maximum crosscorrelation coefficient between the two seismograms is about only 0.38 at a lag of 4.1. The drift time between them is calculated by equations 13-15 with knowledge of Q and is shown in blue in the bottom panel of Figure 8, in which the drift time estimated by DTW is plotted in red. The estimated drift time well approximates the trend of the theoretical drift time but looks unrealistically jittery. Using equation 2, the stationary seismogram is corrected by the theoretical and the estimated drift time respectively (Figure 9). In either way, the corrected stationary seismogram has a drastically increased maximum cross-correlation coefficient of 0.87 and 0.84 at a decreased lag of 0.6 and 0.5 respectively in comparison with the nonstationary one. However, the waveforms embedded in the latter one appear abrupt due to the trembling in the estimated drift time curve.

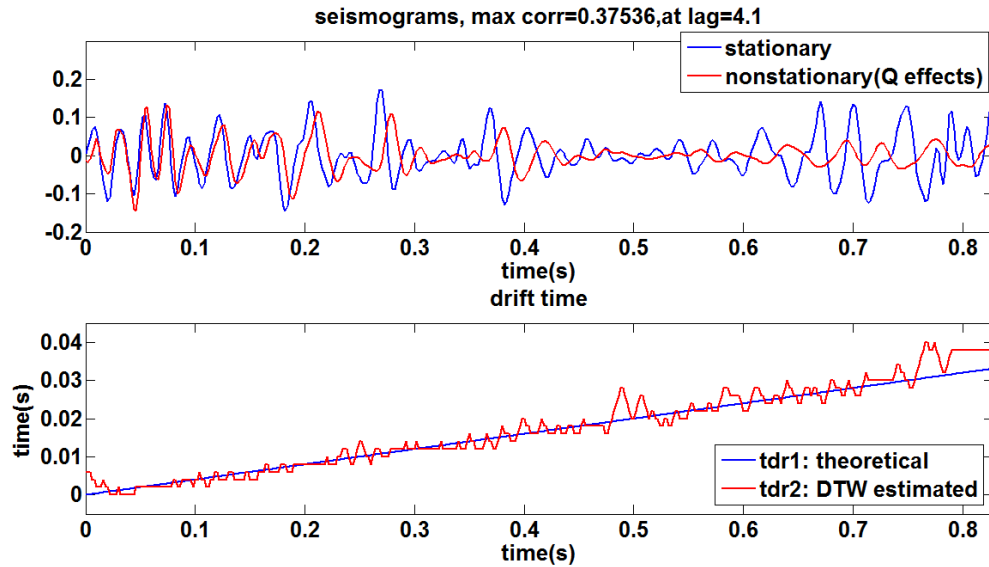


FIG 8: The stationary seismogram created by stationary convolution and the nonstationary seismogram which is the leftmost trace of figure 7 (top). The drift time sequences calculated in theory and estimated by DTW (bottom).

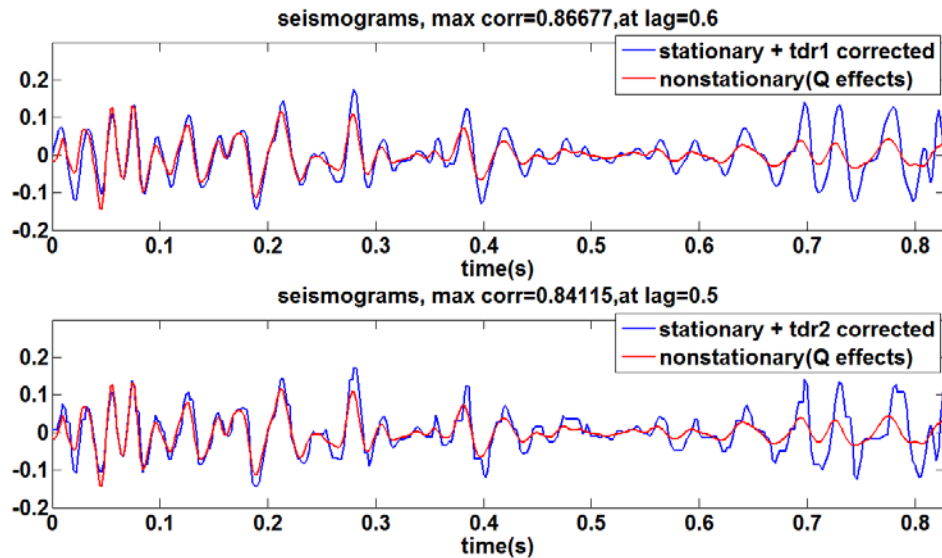


FIG 9: The stationary seismogram corrected by the theoretical drift time compared to the nonstationary seismogram (top). The stationary seismogram corrected by the DTW estimated drift time compared to the nonstationary seismogram (bottom).

The drift time sequence estimated by DTW can be further constrained by changing equation 6 to

$$\sum_{k=1}^b |u(n-k+1) - u(n-k)| \leq 1. \quad (16)$$

In words, the warping path to the optimization problem described by equations 4 and 5 is constrained to the lag sequences in blocks of b samples. Equations 6, 9, and 11 are

corresponding $b = 1$. In the case of $b = 2$, equations 8 and 9 in the accumulation step are changed to

$$d(m,1) = e(m,1), \quad (17)$$

$$d(m,2) = e(m,2) + \min \begin{cases} d(m-1,1) \\ d(m,1) \\ d(m+1,1) \end{cases}, \quad (18)$$

$$d(m,n) = e(m,n) + \min \begin{cases} e(m-1,n-1) + d(m-1,n-2) \\ d(m,n-1) \\ e(m+1,n-1) + d(m+1,n-2) \end{cases}, \quad n = 3, 4, \dots, N. \quad (19)$$

Accordingly, equations 10 and 11 in the backtracking step are replaced by

$$u(N) = \arg \min_{-L \leq m \leq L} d(m, N) \quad (20)$$

$$u(n) = \arg \min_{m \in \{u(n+1)+1, u(n+1), u(n+1)-1\}} d(m, n), \quad n = N-1, N-2, \dots, 1. \quad (21)$$

$$u(n-1) = u(n), \text{ if } u(n) \neq u(n+1)$$

Similarly, equations in the accumulation and backtracking steps should be changed according to different values of b (Hale, 2013).

To test which value of b can estimate the drift time by DTW to maximize the correlation between the corrected stationary seismogram and the nonstationary one, a series of b values ranging from 1 to 415 with the interval of 1 is applied in the DTW algorithm individually since the seismogram has 415 samples. For each value of b , the maximum crosscorrelation coefficient between the corrected stationary seismogram and the nonstationary one is calculated and shown in Figure 10. Panel a) is the maximum crosscorrelation coefficient for each value of b and panel c) is the corresponding lag where the coefficient is maximum. Panel b) and panel d) are the zoomed-in versions of them. We can observe that when b ranges from roughly 5 to 25, the coefficient is prominently high and the corresponding lag is remarkably low among the 415 values.

In Figure 11, the top panel shows the drift time estimated by DTW when b equals 1, 10 and 30 respectively in comparison with the theoretical drift time. Accordingly, the bottom panel shows the stationary seismograms corrected by the corresponding drift time compared to the nonstationary seismogram. We can see a lower value of b causes the trembling in the drift time sequence for lack of constraints in DTW while a higher value underestimates the drift time because the constraint is too strict, and both cases will decrease the correlation between the corrected stationary seismogram and the nonstationary seismogram. Thus, 10 is chosen as the value of b for drift time estimation and correction in our example.

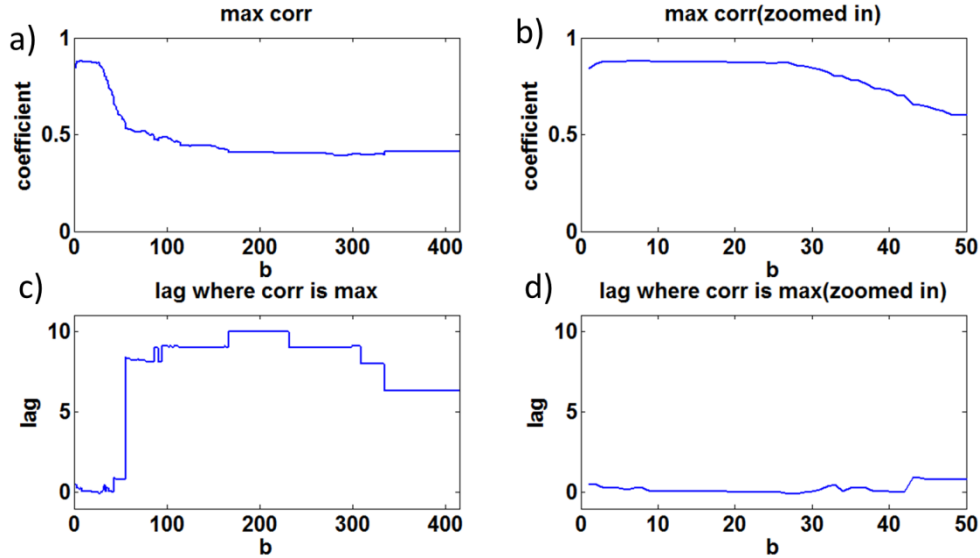


FIG 10: Maximum crosscorrelation coefficient (a and b) and the corresponding lag (c and d) between the nonstationary seismogram and the stationary one corrected by DTW estimated drift time using every possible b value.

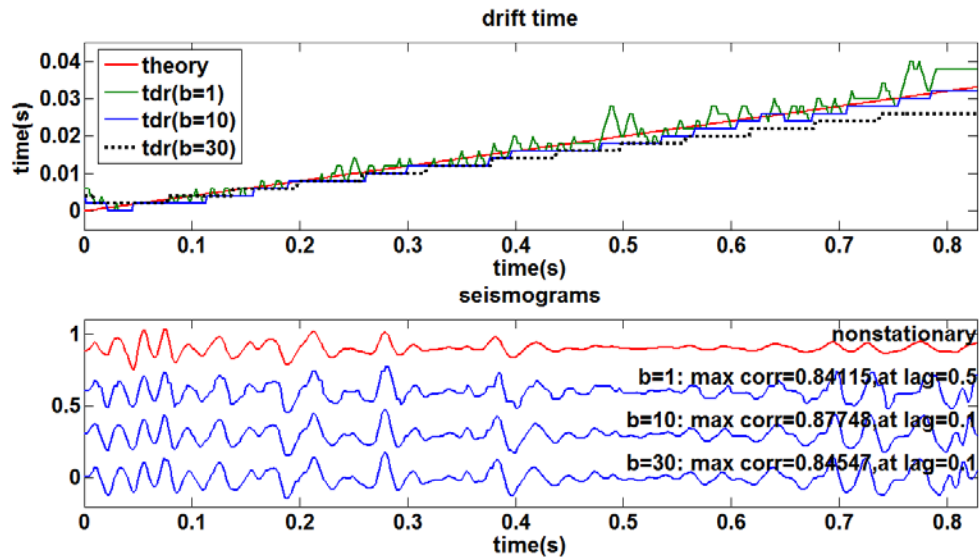


FIG 11: The drift time estimated by DTW when b equals 1, 10 and 30 in comparison with the theoretical drift time (top). The stationary seismograms corrected by the corresponding drift time in the top panel compared to the nonstationary seismogram (bottom).

Matching perfection

Although the crosscorrelation coefficient between the nonstationary seismogram and the stationary one has increased from 0.38 (Figure 8 top panel) to 0.88 after correction by the DTW estimated drift time using $b = 10$ (the green curve in Figure 11 bottom panel), there is still visible time-variant amplitude imbalance between them (the red and green curves in Figure 11 bottom panel) as well as possible residual phase.

To further increase the correlation, a time-variant amplitude balancing is applied to the nonstationary seismogram with respect to the corrected stationary one using 0.1 s Gaussian windows with 0.002 s increment as shown in Figure 12 top panel and the maximum crosscorrelation has reached 0.93. Next, a time-invariant and a time-variant (using the same Gaussian windows as the time-variant amplitude balancing) constant-phase difference are detected individually between the two seismograms and shown in Figure 12 bottom panel. The time-invariant phase is -3 degrees, approximately the average value of the time-variant phases which are almost constant with time. Finally, the balanced nonstationary seismogram is rotated by the two phase differences and is compared with the corrected stationary seismogram respectively in Figure 13. We can observe that very similar matching results are got by the time-invariant and time-variant constant-phase rotations.

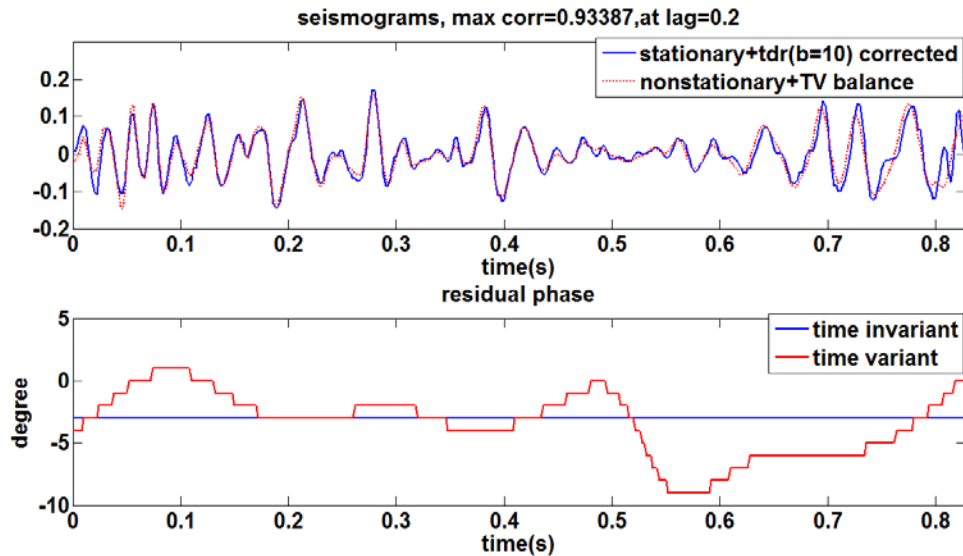


FIG 12: The nonstationary seismogram after the time-variant amplitude balancing in comparison with the drift time corrected stationary one (top). The time-invariant and time-variant constant-phase differences between the seismograms of the top panel (bottom).

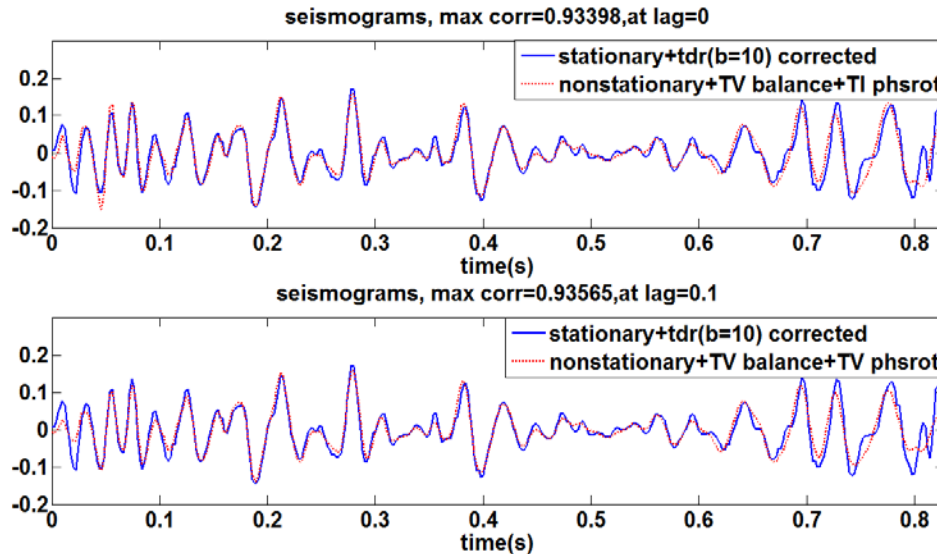


FIG 13: Final matching of the two seismograms after the time-invariant constant-phase rotation (top) and the time-variant constant-phase rotation (bottom).

DISCUSSION

Effect of internal multiples

A more realistic 1D seismogram containing internal multiples is constructed by the VSP algorithm based on the same well log, wavelet and Q value. Figure 14 shows the upgoing wavefield of the synthetic zero offset VSP with both Q and internal multiple effects. The leftmost trace is plotted in red in Figure 15 top panel compared to the stationary seismogram in blue and the nonstationary one in green with only Q effects. We can observe that the events in the nonstationary seismogram with both Q and internal multiple effects appear more decay in the amplitude and more delay in the traveltimes with comparison to the one with only Q effects. The drift time of the two nonstationary seismograms with respect to the stationary one is estimated individually by DTW using $b=10$ and is shown in Figure 15 bottom panel in comparison with the theoretical drift time calculated from $Q=50$. Apparently, the drift time estimated from the nonstationary seismogram including both Q and internal multiple effects is progressively higher than the theoretical one, indicating a smaller value of Q than 50. As first discussed by O'Doherty and Anstey (1971), short-path multiples cause a nonstationary filtering effect that is essentially indistinguishable from anelastic attenuation and has come to be called stratigraphic filtering. Combination of both anelastic attenuation and stratigraphic filtering leads to a single combined effect that can be modelled by the constant Q theory (Kjartansson, 1979) as an apparent Q , whose value is lower than the intrinsic Q caused by anelastic attenuation alone (Margrave, 2013). Thus, the drift time between the nonstationary seismogram containing both Q and internal multiple effects and the stationary one is caused by the apparent Q whose value is smaller than the intrinsic Q value of 50.

In Figure 16 top panel, the stationary seismogram is corrected by drift time estimated from the nonstationary seismogram with both Q and internal multiple effects, which is then time-variant balanced and time-variant constant-phase rotated with respect to the

corrected stationary seismogram shown in Figure 16 bottom panel. The final matching obtains a maximum crosscorrelation coefficient of 0.93 at a lag of 0.1.

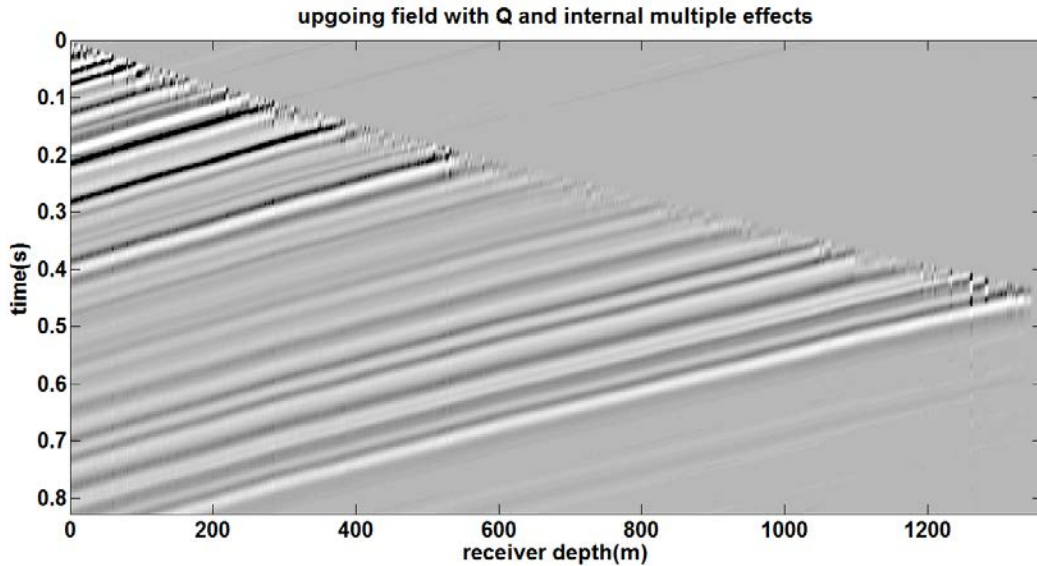


FIG 14: The upgoing wavefield for the VSP modelling only with primaries and internal multiples.

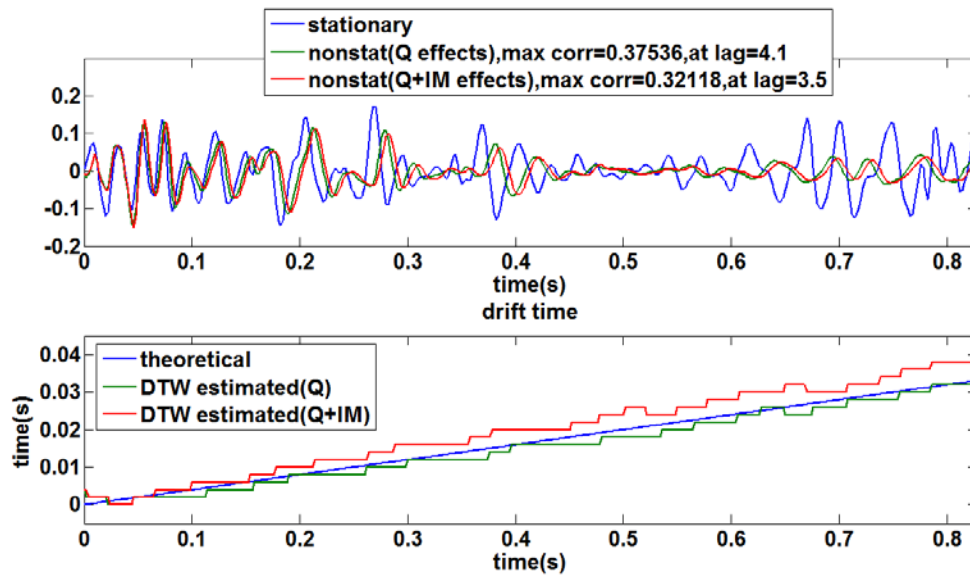


FIG 15: The stationary seismogram, the nonstationary seismogram only with Q effects and the nonstationary seismogram with both Q and internal multiple effects (top). The drift time sequences calculated in theory and estimated from the two nonstationary seismograms in the top panel by DTW (bottom).

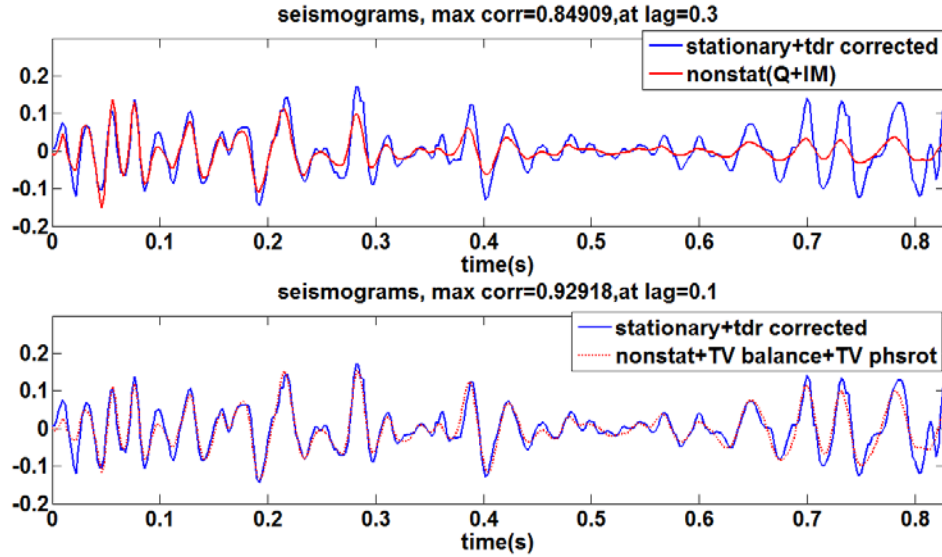


FIG 16: Drift time corrected stationary seismogram in comparison to the nonstationary seismogram (top) and time-variant balanced and time-variant phase rotated nonstationary seismogram (bottom).

Wavelet estimation

In the previous cases, all the stationary seismograms, which are to be drift time corrected, are created using the known minimum-phase wavelet of Figure 6. In the practical procedure of well tying, the wavelet embedded in the nonstationary seismic trace is always unknown and needs to be estimated from the trace. For simplicity, the nonstationary seismogram with Q effects only (see red curve in Figure 8 top panel) is used to test drift time estimation by DTW with an estimated wavelet.

The amplitude spectrum of an average wavelet across the whole nonstationary seismogram is estimated by the statistical wavelet estimation method (Cui and Margrave, 2014) with a desired wavelet length of 0.2 s, which is controlled by a Gaussian window. As is shown in Figure 17 top panel, the dominant frequency of the estimated wavelet is lower than the known wavelet, because the known wavelet does not contain any Q attenuation while the estimated wavelet is an average over a series of progressively attenuated wavelets. In Figure 17 bottom panel, the wavelet in red is the same minimum-phase wavelet as in Figure 6; the one in blue is estimated with a constant-phase of zero supplied; the one in green is estimated with a minimum-phase supplied. The minimum-phase $\varphi_m(f)$ is calculated by

$$\varphi_w(f) = H(\ln(|W(f)|)), \quad (22)$$

where $|W(f)|$ is the amplitude spectrum of the wavelet and H denotes the Hilbert Transform (Margrave, 2013).

Next, either of the estimated wavelets is convolved with the reflectivity (Figure 5) to construct a corresponding stationary seismogram, which is shown in Figure 18 top panel in comparison with the time-variant balanced nonstationary seismogram respectively.

The maximum crosscorrelation coefficients between the nonstationary seismogram and the two stationary seismograms are both about 0.28 but at difference lags, whose value is 36.4 in the zero-phase case and 3.2 in the minimum-phase case. Then the drift time sequence between either of the stationary seismograms and the nonstationary one is estimated by DTW with $b=10$ and is shown in Figure 18 bottom panel, where we can observe a time shift between the two estimated drift time sequences.

With the drift time estimated, either of the two stationary seismograms is corrected accordingly in Figure 19 top panel in contrast with the time-variant balanced nonstationary seismogram. The maximum cross-correlation coefficient has increased to 0.9 at a decreased lag of 0.8 in the minimum-phase case while in the zero-phase case, it has increased to 0.7 at a decreased lag of 0.7. Thus, the lag difference in Figure 18 top panel is almost compensated by the time shift between two drift time sequences in Figure 18 bottom panel. To perfect the matching, a time-variant constant-phase difference is detected between the time-variant balanced nonstationary seismogram and either of the stationary seismograms. As Figure 19 bottom panel shows, the phase difference is slight and nearly constant in time for both cases. Then the constant-phase difference is applied to the time-balanced nonstationary seismogram correspondingly and the final maximum crosscorrelation coefficient is 0.8 at a lag of 0.3 in the zero-phase case and 0.9 in the minimum-phase case at a lag of -0.2, which are very similar results.

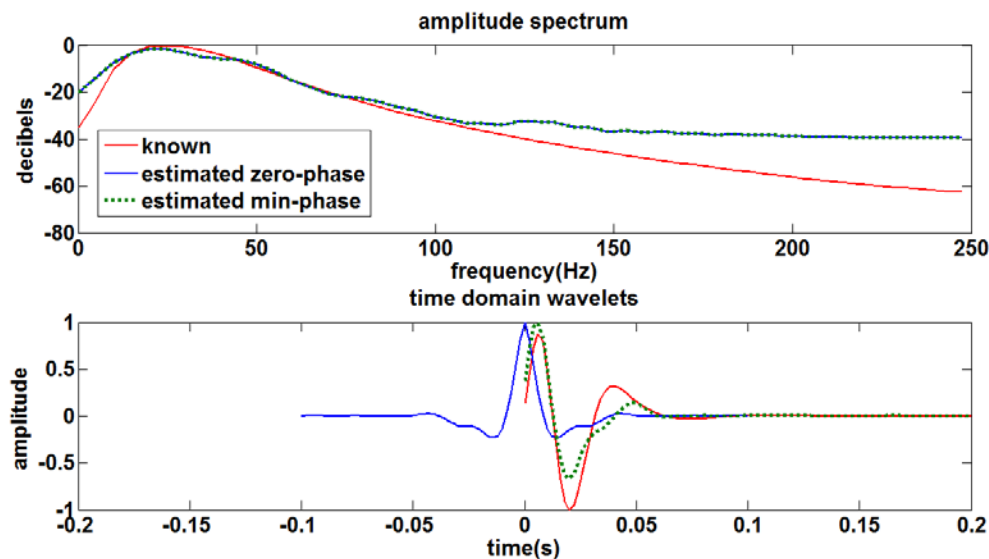


FIG 17: The amplitude spectra in decibels (top) and the time domain waveforms (bottom) of the known minimum-phase wavelet, the estimated zero-phase wavelet and the estimated minimum-phase wavelet.

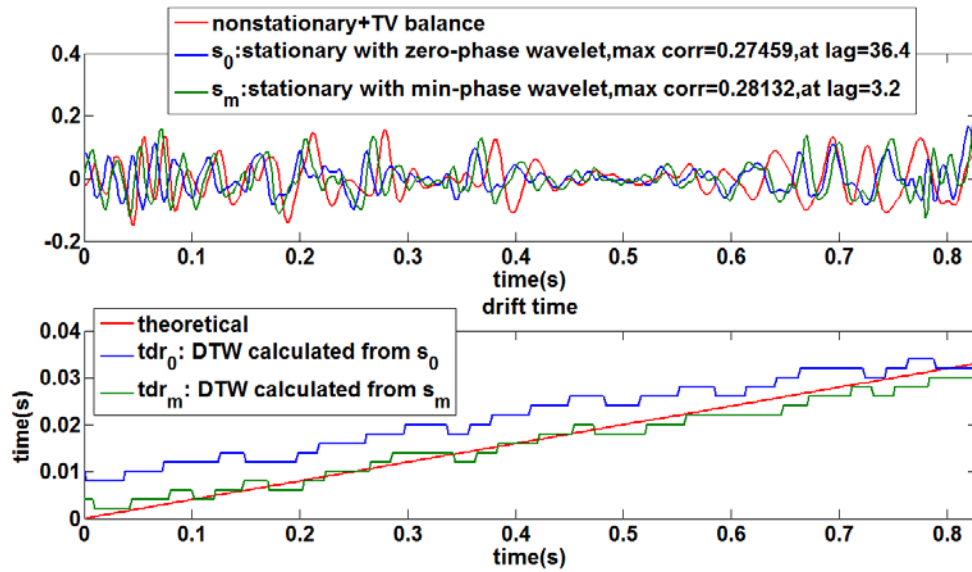


FIG 18: Stationary seismograms created by the estimated zero-phase and minimum-phase wavelets in comparison with the time-variant balanced nonstationary seismogram (top). Drift time sequences estimated by DTW from the two stationary seismograms compared with the theoretical drift time calculated using a Q value of 50 (bottom).

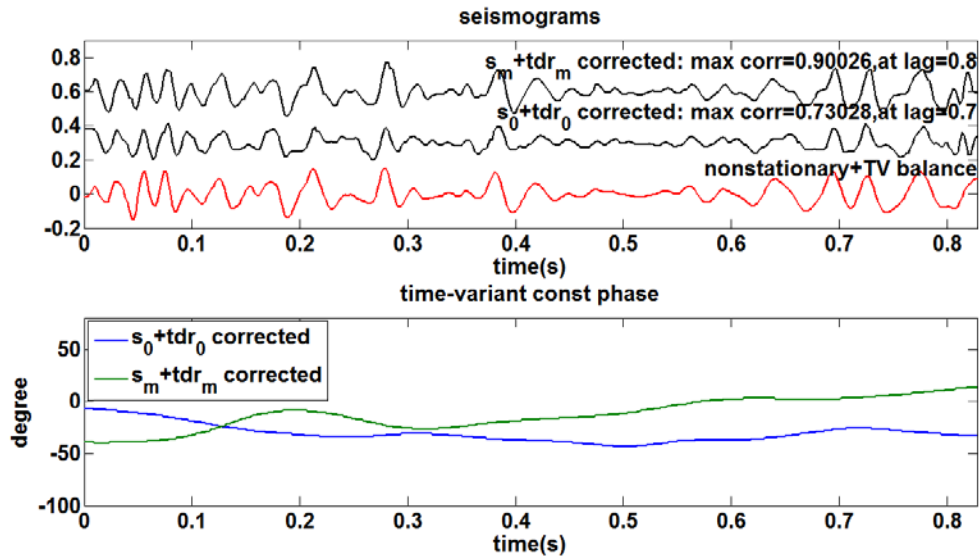


FIG 19: Drift time corrected stationary seismograms created by the estimated zero-phase and minimum-phase wavelets compared to the time-variant balanced nonstationary seismogram (top). The time-variant residual constant-phase in the time-variant balanced nonstationary seismogram with respect to either of the drift time corrected stationary seismograms (bottom).

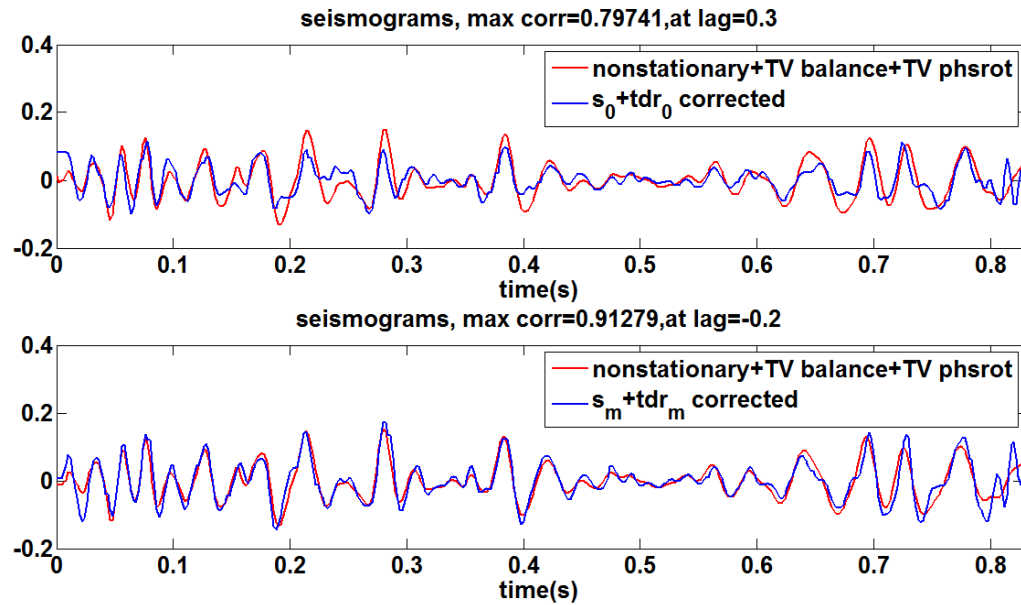


FIG 20: Final matching of the stationary seismograms created by the estimated wavelets with the nonstationary seismogram with Q effects only.

Necessity of drift time correction

Suppose the stationary seismograms created by the estimated wavelets in Figure 18 top panel will not be drift time corrected. Figures 21 and 22 test the matching of the stationary and nonstationary seismograms only by the time-variant amplitude balancing (0.1 s Gaussian windows with 0.002 s increment) and the time-invariant or the time-variant (the same Gaussian windows as the time-variant balancing) constant-phase rotation. Figure 21 shows the final matching in the zero-phase case, where there is a large residual constant-phase in the time-variant balanced nonstationary seismogram which also varies drastically in time. Although the time-variant constant-phase rotation works better than the time-invariant one, there are still mismatches compared to the case in which drift time correction is applied (Figure 20 top panel). Similar conclusions can be also drawn in the minimum-phase case as shown in Figure 22 and Figure 20 bottom panel.

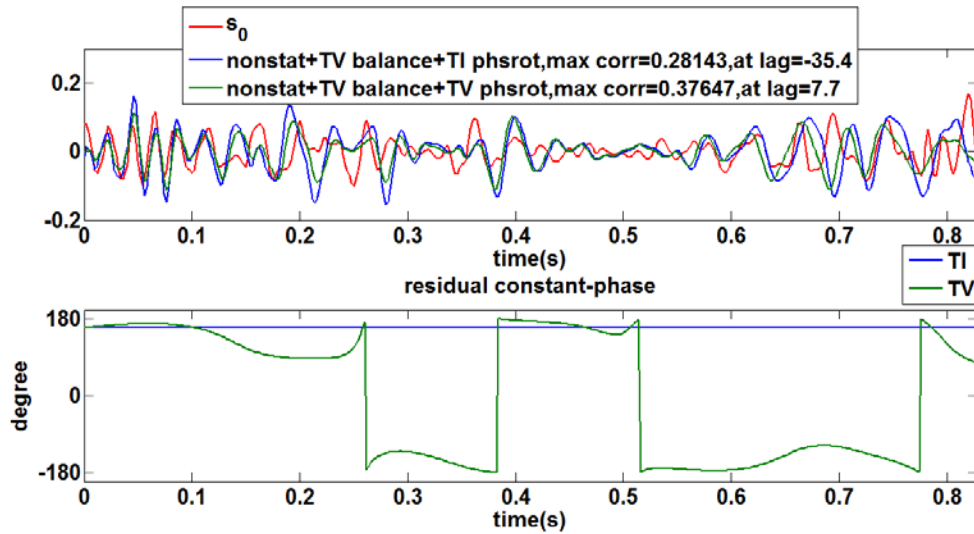


FIG 21: Matching the stationary seismogram created by the estimated zero-phase wavelet and the nonstationary seismogram only using the time-variant amplitude balance and the time-invariant or the time-variant constant-phase rotation.

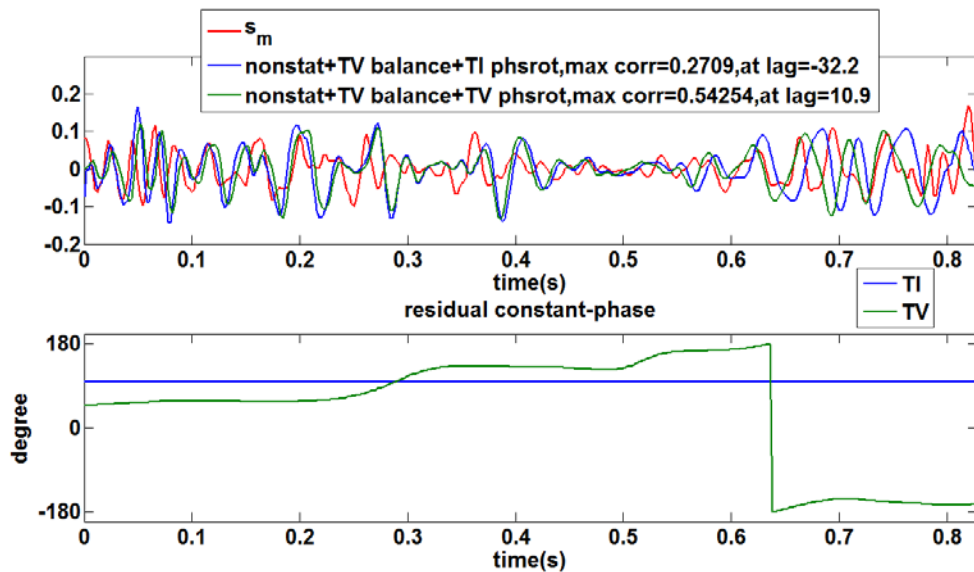


FIG 22: Matching the stationary seismogram created by the estimated minimum-phase wavelet and the nonstationary seismogram only using the time-variant amplitude balance and the time-invariant or the time-variant constant-phase rotation.

CONCLUSIONS

Based on the constrained optimization algorithm, dynamic time warping is a fast and automatic method to estimate the drift time between the stationary synthetic seismogram and the nonstationary seismic trace with attenuation by matching the two seismograms, without knowledge of Q or check-shot records. Parameter b should be tested to get an accurate estimation. When nonstationarity of the seismic trace is only caused by anelastic attenuation, the drift time estimated by DTW can closely approximate the theoretical drift time calculated from the intrinsic Q value. When the nonstationary seismic trace resulted from both anelastic attenuation and stratigraphic filtering, DTW estimates the drift time

associated with the apparent Q , which has a positive time shift compared to the former one. If the stationary seismogram is constructed by a statistically estimated wavelet from the nonstationary seismogram but with an incorrect phase, DTW can compensate the phase difference by estimating a time shift sequence with the combined effect of both drift time and extra time shift associated with the phase difference.

The matching of the stationary and nonstationary seismograms can be perfected by time-variant amplitude balancing and constant-phase rotation following the drift time correction. The residual constant-phase between the drift time corrected stationary seismogram and the time-variant balanced nonstationary seismogram is small and almost constant in time, whereas it varies in a large range between the stationary seismogram without drift time correction and the time-variant balanced nonstationary seismogram. Thus, by applying drift time correction, the phase difference between the stationary and nonstationary seismograms become more constant in both time and frequencies, which both time-variant and time-invariant constant-phase rotations can correct the residual phase. On the contrary, without drift time correction, the time-variant constant-phase rotation is insufficient to correct the time and frequency dependent phase difference caused by attenuation as well as the incorrect phase of the estimated wavelet. So drift time correction is a necessary procedure to tie the stationary synthetic seismogram to the nonstationary seismic trace.

ACKNOWLEDGEMENTS

We thank the sponsors of CREWES for their support. We also gratefully acknowledge support from NSERC (Natural Science and Engineering Research Council of Canada) through the grant CRDPJ 379744-08.

REFERENCES

- Cui, T. and Margrave, G. F., 2014, Seismic wavelet estimation, in the 26th Annual Report of the CREWES Project.
- Hale, D., 2013, Dynamic warping of seismic images: *Geophysics*, 78(2), S105-S115.
- Kjartansson, E., 1979, Constant Q -wave Propagation and Attenuation, *Journal of Geophysical Research*, 84, 4737-4748.
- Margrave, G. F., 2013, Methods of seismic data processing – *Geophysics 517/557 Course Notes: The Department of Geoscience, University of Calgary*.
- Margrave, G. F., 2013, Q tools: Summary of CREWES software for Q modelling and analysis, in the 25th Annual Report of the CREWES Project.
- Margrave, G. F., 2013, Why seismic-to-well ties are difficult, in the 25th Annual Report of the CREWES Project.
- O'Doherty, R. F., and Anstey, N. A., 1971, Reflections on amplitudes, *Geophysical Prospecting*, 19, 430-458.